ELSEVIER

Surface Science 421 (1999) 1–16

surface science

Hydrogen on the Fe(110) surface and near bulk bcc Fe vacancies A comparative bonding study

Alfredo Juan [1], Roald Hoffmann *

Department of Chemistry and Materials Science Center, Cornell University, Ithaca, NY 14853-1301, USA

Received 17 May 1998; accepted for publication 22 September 1998

Abstract

The bonding of H to Fe is analyzed using qualitative band structure calculations in the framework of extended Hückel tight-binding theory and the ASED-MO cluster method. The changes in the electronic structure of bcc Fe upon the introduction of H at a vacancy are addressed, and a comparison drawn with H adsorption at the Fe(110) surface. H in bulk Fe with vacancies prefers a tetrahedral site shifted toward the vacancy. The vacancies act as a strong trap for H. The Fe atoms are initially more strongly bonded to each other as a consequence of vacancy formation; their Fe–Fe bond strength is then diminished as the new Fe–H bond is formed. The effect of H is limited to its first Fe neighbor. An analysis of the orbital interactions reveals that the Fe–H bonding involves mainly the Fe 4s and H 1s orbitals with less participation of Fe 4p and 3d crystal orbitals. Relaxation of Fe atoms neighboring the vacancy is also addressed. A detailed atomistic mechanism for decohesion and H embrittlement is provided.

Keywords: Electronic structure; Embrittlement; Fe(110); Hydrogen; Molecular orbitals; Vacancy

1. Introduction

There are good reasons to look at hydrogens at the surface and inside metals. Hydrogen–defect interactions in metals, semiconductors and alloys influence many important material properties [1]. The practical uses of metal–hydrogen systems include the ability of some metals and alloys to store hydrogen, as well as the very important catalytic properties of transition metal surfaces in hydrogenation reactions. There are also undesired effects of small amounts of hydrogen in metals on important material properties. Impurities such as H, present in a few parts per million, can result in a dramatic decrease in plasticity and drastic degrading of mechanical properties by crack propagation and corrosion [2–4].

Hydrogen is the smallest interstitial inside a metal, so it can diffuse very rapidly. However, a mechanism for hydrogen embrittlement has not been unequivocally established [4,5]. Besenbacher et al. have suggested a way to mitigate this metallurgical problem: perhaps one could modify the H transport rate by trapping it at defects, instead of allowing H to accumulate at potential fracture sites such as grain boundaries (GB) or crack tips [6]. One of the first suggestions of diffusing H captured by lattice traps was made by Oriani [7].

The solubility of H in Fe is less than

* Corresponding author. Fax: +1 607 255 5707; e-mail: rh34@cornell.edu

[1] Permanent address: Dpto. Física, Universidad Nacional del Sur, Av. Alem 1253, 8000 Bahía Blanca, Argentina.

0039-6028/99/$ – see front matter
PII: S0039-6028(98)00780-8

10^{-6} atom H/atom Fe at room temperature and 1 atm of H_2 gas [8]. A stable hydride is only formed at pressures ~ 6.7 GPa and $T = 250°C$; it has a double hcp structure (dhcp) [9]. The stacking sequence of closest packed layers for dhcp follows the pattern ABAC, with *c*-axis twice the length of the hcp AB stacking, where A, B and C represent the three possible orientations of the layers.

Experimental work on the H–bcc Fe system in the solid state is scarce; the low solubility of H and its high mobility make direct observations extremely difficult. Griessen has developed a local semi-empirical correlation (based on thermodynamic and crystallographic data and on the electronic structure of metals) that reproduces remarkably well the experimental values of the heat of hydrogen solution in transition metals at infinite dilution, the volume expansion after H absorption, and the correct site occupancy [10].

While numerous theoretical calculations of the electronic structure of H in transition metals containing defects have been carried out [1], the H–Fe system has not been as extensively studied as H in other metals [11–18]. Adachi and Imoto, using ab initio quantum chemical methods and small fcc cluster models, presented a systematic interpretation of the electronic properties of H in transition metals [19]. Opitz et al. have proposed a uniform bonding mechanism for interstitial hydrogen in 3d transition metals that explains how the metal–metal bond is weakened as the metal–hydrogen bond is formed [14]. Atomistic simulation using embedded atom interatomic potentials has been developed for H in transition metals, including Fe and intermetallic alloys [20]. Minot and Demangeat have investigated (by extended Hückel calculations) the lattice localization of hydrogen as an interstitial in bcc Fe. They found the solution of H in Fe strongly endothermic, with a preference for H tetrahedral site occupancy and charge transfer from the H atom to the neighbor metal atoms [21].

The occurrence of H trapping at vacancies has been experimentally demonstrated for a number of metals. In the absence of H, vacancies previously produced disappear when the temperature is sufficiently high for them to become mobile. When H is present in metals, the H–vacancy complex reduces that mobility [1–4]. Substantial insight into the microscopic nature of the trapping mechanism in vacancies has emerged from a combination of experiment and effective medium theory [6]. A theoretical analysis of hydrogen interaction with metals, including chemisorption, interstitials, defects and hydride formation, was given by Nordlander et al. [12]. Among the few experimental studies on the H–Fe vacancy complex, we can cite that of the induced equilibrium vacancies in Fe and fcc Fe base alloys [22–24] and the characterization of the defect complex by positron annihilation [25].

The vacancy–hydrogen interaction and hydrogen pairing in some transition metals have been studied previously using first principles calculations on cluster models, effective medium theory, tight-binding and ASED-MO calculations [26–31]. Recently, Itsumi and Ellis have reported first principles electronic structure calculations for bcc Fe_{32} clusters with and without H, and also involving a vacancy. These authors predict Fe–Fe bond weakening due to H located in an octahedral site shifted toward the vacancy [32].

The main objective of the present work is to provide a comparison between H absorption near an Fe vacancy and chemisorption on an Fe(110) surface. A vacancy generates an interior surface, albeit a tightly constrained one. What similarities or differences are there between chemisorption at a surface and binding in a cavity in the interior of the metal? Our study begins to explore these questions.

The tight-binding extended Hückel method is employed to trace the relevant orbital interactions and to discuss the electronic consequences of incorporating H on Fe–Fe bonding. The theory and the models are considered in the next sections.

2. Theoretical method

Our calculations were performed using the tight-binding extended Hückel (EH) method [33–35], an approximate molecular orbital scheme, implemented with the YAeHMOP program [36]. Double zeta expansions of the metal d orbitals were employed; the parameters are listed in

Table 1
Extended Hückel parameters

Atom	Orbital	H_{ij} (eV)	ξ_1	ξ_2	c_1	c_2
H	1s	13.600	1.30			
Fe	4s	7.870	1.70			
	4p	4.104	1.40			
	3d	9.000	5.35	1.80	0.5366	0.6678

Table 1. The off-diagonal Hamiltonian matrix elements were computed with the modified Wolfberg–Helmholtz formula [37]. For slab calculations an 18k point set was generated according to the geometrical method of Ramirez and Böhm [38,39]. To test the convergence, a mesh of 64k points was used in several cases, and no differences were observed. In the case of bulk bcc Fe, a 220k point set was employed.

The energies and optimized positions for H are taken from experimental data or computed with a cluster approximation using the ASED-MO method, which is a modification of the EH method that includes repulsive terms in the energy [40]. This method evaluates the electrostatic force acting on the nuclei, that force being a function of the charge distribution. The adsorption (absorption) energy is defined as the difference in energy between the H–Fe composite system when the H is chemisorbed (absorbed) at a specified geometry and when it is removed from the Fe surface (bulk). For the ASED-MO method, the total energy difference can be expressed as:

$$\Delta E_{\text{total}} = E(\text{H–Fe}_n) - E(\text{Fe}_n) - E(\text{H}) + E_{\text{repulsion}}$$

where E is the electronic energy and n the size of the cluster. The repulsion energy ($E_{\text{repulsion}}$) of nucleus B in the presence of a fixed atom A is calculated from:

$$E_{\text{repulsion}} = \tfrac{1}{2} \sum_{\text{A}} \sum_{\text{B}\neq\text{A}} E_{\text{AB}}$$

where E_{AB} is a pairwise electrostatic energy term. The summation is extended over all Fe–Fe and H–Fe pairs [40].

Although the EH method is quite approximate, the analysis of orbital interactions by this technique seems to be reasonably reliable. The strength of EH is in fact its transparency, not accuracy, and the main objective of this work is to provide a qualitative picture of H adsorption on the surface and binding within Fe. The method allows us to determine the contribution of each orbital of Fe and H to the bonding. Throughout this paper, two conceptual tools — density of states (DOS) and crystal orbital overlap population (COOP) curves — are used extensively to shed more light on the H–Fe interaction. The DOS curve is a plot of the number of orbitals per unit volume per unit energy. The COOP curve is a plot of the overlap population weighted DOS vs. energy. Integration of the COOP curve up to the Fermi level (E_{f}) gives the total overlap population of the bond specified. Looking at the COOP, we may analyze the extent to which specific states contribute to a bond between atoms or orbitals [41].

3. Models for the Fe vacancy, the Fe(110) surface, and their interaction with H

α-Iron has a bcc structure with $a = 2.861$ Å and a nearest neighbor distance of 2.47 Å [42]. The (110) face is centered rectangular; to describe it we used a C(4 × 4) unit cell. The thickness of the α-Fe(110) slab should be such that it approximates the electronic structure of 3D bulk Fe in the innermost layer. In order to achieve the best compromise between computational time and accuracy of our model, we chose to use a seven layer slab. The unit cell of ${}^{2}_{\infty}[\text{Fe}_{56}]$ is shown schematically from the top in Fig. 1. The interlayer spacing in this Fe(110) model is 2.02 Å. Our slab has two identical surface-like layers and five inner layers. A side view of a section of the unit cell showing the Fe coordination, the localization of the vacancy, and the interstitial sites can be seen in Fig. 2.

A test of the adequacy of our choice of slab thickness is shown in Fig. 3. Curve (a) is the DOS for 3D bulk Fe, while (b) corresponds to the DOS of the innermost (fourth) layer, and (c) shows one of the surface layers. Note that the fourth slab layer reproduces very well the DOS of bulk Fe.

We proceed to construct a H adsorption model near an Fe bulk vacancy, and then the model for

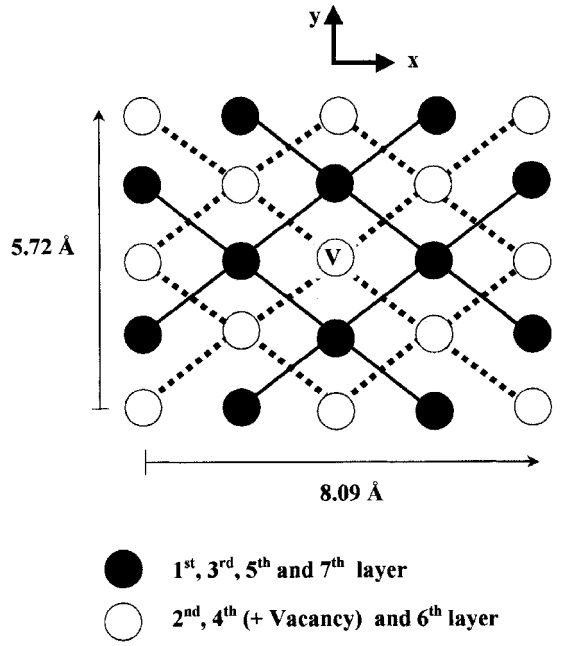

Fig. 1. Schematic "top" view of the unit cell used $^{2}_{\infty}[Fe_{56}]$.

H chemisorption on the Fe(110) surface. In both cases, similar Fe slabs were used. However, before we do so, it is useful to define in some detail the interstitial sites in the bcc lattice.

The bcc lattice has two interstitial sites commonly called "tetrahedral" and "octahedral". As Scheme 1 shows, neither site is an ideal Platonic polyhedron environment. Thus, in the tetrahedral site the distances between the surrounding Fe atom vertices are $a\sqrt{3}/2$ (four such) and a (two). The octahedral site is also bounded by Fe atoms separated $a\sqrt{3}/2$ (eight such pairs) and a (four).

3.1. H near an Fe bulk vacancy

The Fe bulk vacancy is placed exactly at the center of the unit cell (see Fig. 2) and the H is located in the vacancy region at the position of lowest energy found in a previous study [30]. This corresponds to a so-called tetrahedral interstitial site (formed by Fe_{1V}, Fe_{3V}, Fe_{4V}, and the vacancy V in Scheme 2 and Fig. 2), but with the H displaced further, by 0.25 Å toward the vacancy vertex. The H–third layer distance is 0.81 Å, and the closest H–Fe distance in this configuration is

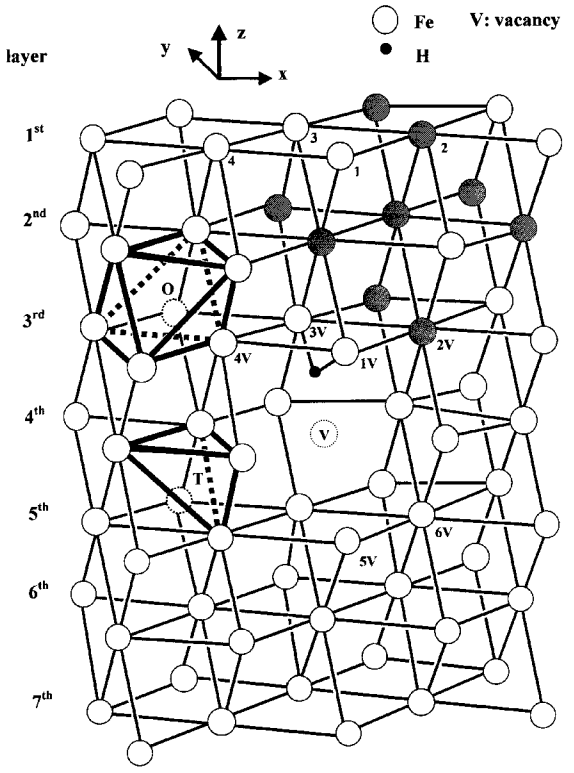

Fig. 2. Side view of the cell [some atoms are removed to show the vacancy position (in the fourth layer)]. The bulk bcc Fe coordination may be seen in the shaded atoms. The hydrogen (H) is placed in a tetrahedral interstitial position, near the vacancy. The Fe atoms on the surface (1, 2, 3, 4) and near the vacancy (1V, 2V, 3V, 4V) region are indicated. Tetrahedral (T) and octahedral (O) interstitial sites in the Fe lattice are indicated with thick lines.

1.64 Å (see Scheme 2). We treated lattice relaxation near the vacancy only in a simplified way, by allowing just a breathing mode for the first Fe neighbors.

Hydrogen at tetrahedral or octahedral interstitial sites was also studied in a perfect bcc Fe slab.

3.2. H on Fe(110)

For H adsorption on the Fe(110) surface, a very low coverage model is considered. The H–surface distance is set at 0.90 Å, corresponding to an Fe–H distance of 1.75 Å (see Scheme 3), as determined by LEED [43]. Due to the experimental uncertainty about the preferred adsorption site, a long-

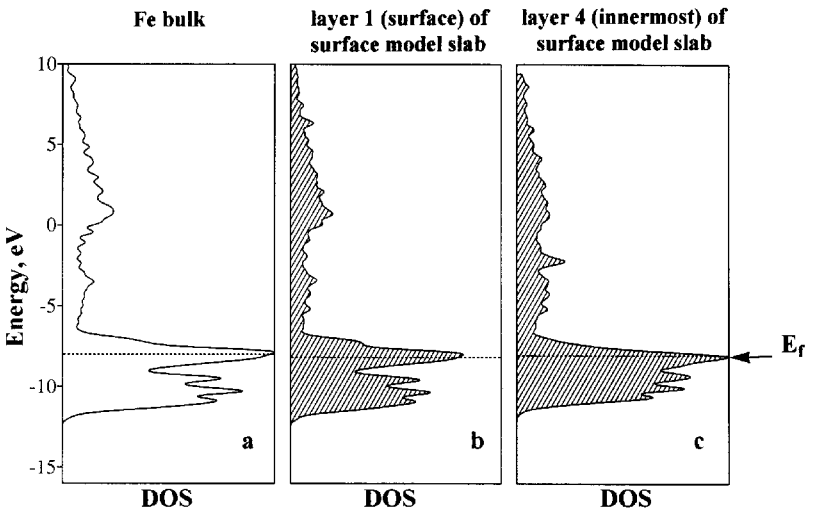

Fig. 3. Total DOS of 3D bulk Fe (a), contribution to the DOS of the innermost layer of atoms (b), and of the surface layer (c) of seven layer slab.

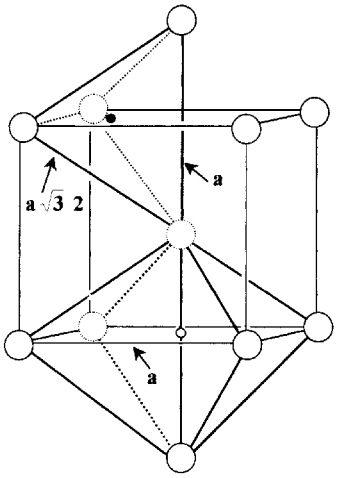

Scheme 1.

bridge position (see Scheme 4) was chosen, as indicated by the theoretical studies of Cremaschi et al. [44]. There is only one H per unit cell, giving a stoichiometry of $^{2}{}_{\infty}[Fe_{56-1}H]$, where -1 represents the removal of a central Fe atom if a vacancy is present. No surface reconstruction or relaxation was considered.

The low H concentration on the surface (and in the vacancy region) was dictated by the necessity of modeling a relatively low solubility of H in bcc Fe, while keeping the thickness of the slab within computationally feasible limits.

4. Results and discussion

Let us discuss first the electronic structure of the innermost (fourth) layer of the Fe slab in the absence of H or any vacancy defect. In the DOS of this bulk-like layer, the metal d states form a band between -12 and -7 eV. A similar band width of ~ 5.0 eV was reported by Griessen [10]. A substantial number of s and p states penetrate the d band. The dispersion of the s and p bands is much larger than the d band, reflecting the more contracted nature of d orbitals. If we look at the detailed composition of, say, the bulk-like (fourth) layer of the slab, we obtain the orbital population $d^{6.74}s^{0.66}p^{0.32}$, which is close to $d^{7.02}s^{0.66}p^{0.32}$ obtained for bulk Fe. Note that on average any Fe atom has its s band approximately 1/3 filled. The calculated value for the Fermi level (E_f)

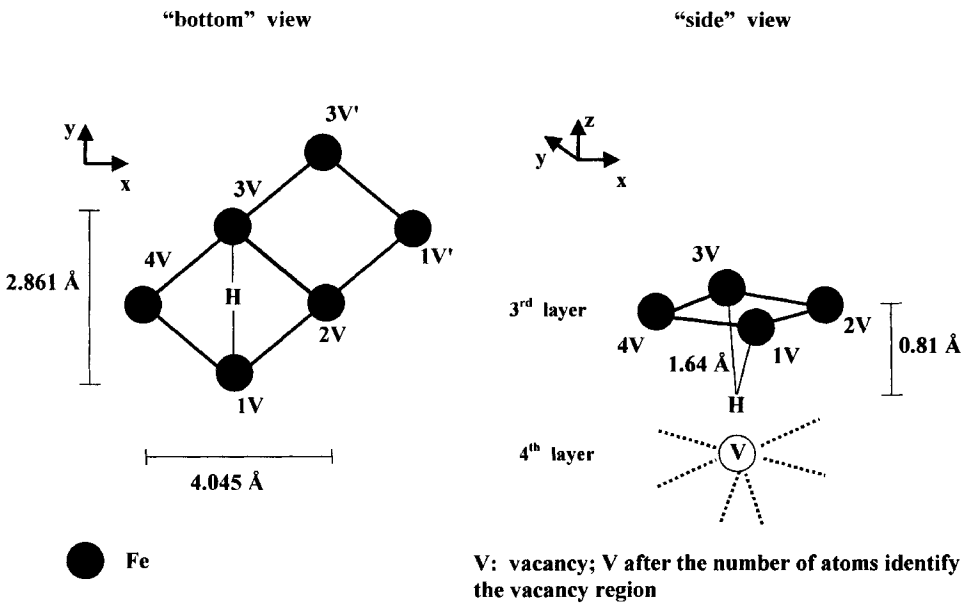

Scheme 2.

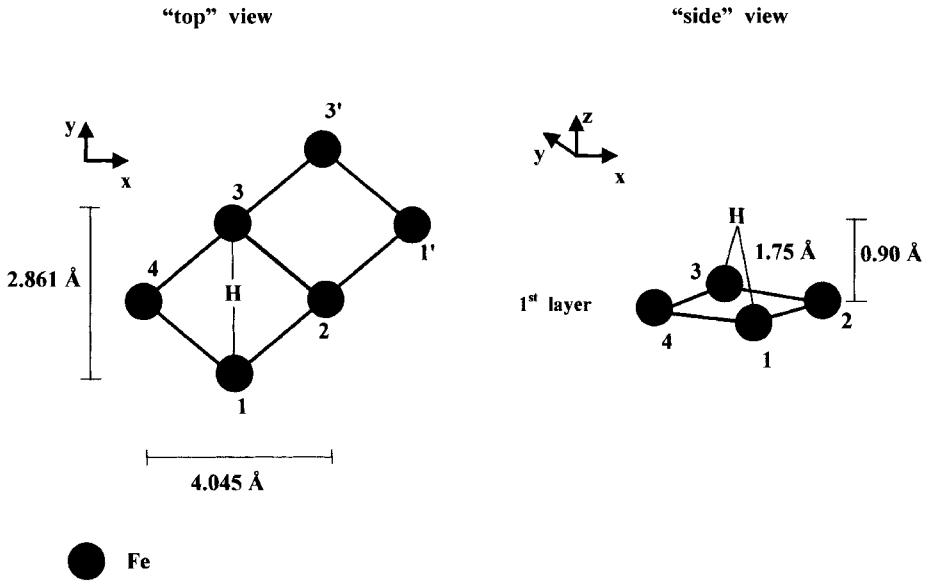

Scheme 3.

exceeds the observed work function for the metal by ~ 3 eV [45], a typical error of the EH method [46]. Our results are in qualitative agreement with those obtained both by experiment and by more sophisticated computational methods [47].

For the two surfaces of the slab, the calculated orbital populations are $d^{7.73}s^{0.70}p^{0.29}$. These layers are negatively charged with respect to the inner layers (see Table 2). This is not unexpected, but has been discussed in detail in a previous paper

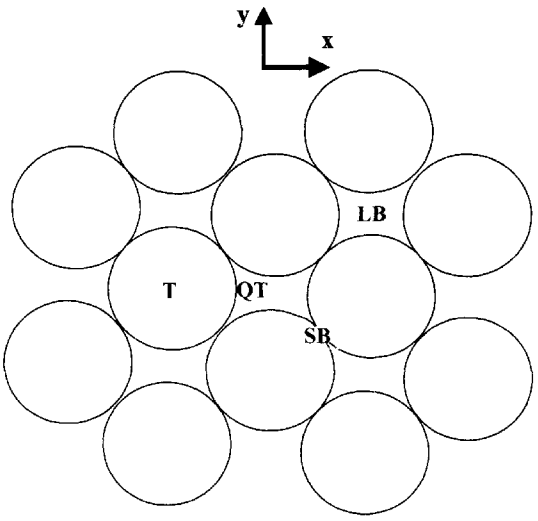

Adsorption positions on Fe(110)

T: Top
LB: Long Bridge
SB: Short bridge
QT: Quasi-three-fold

Scheme 4.

from our group [46], and by others [48–51]. The orbitals of the surface atoms in the surface layers have somewhat less dispersion, i.e. form narrower bands. There are fewer nearest neighbors (six) of a surface atom, compared with the inner atoms (eight): the decrease in coordination reduces the number of overlaps available to an atom and this eventually controls the band width. The DOS decomposition of Fig. 3 shows this effect: the surface atom states are less dispersed and few of them go above the E_f; they are therefore relatively underoccupied.

When a vacancy is introduced into the slab model, the total DOS curve for the slab (Fig. 4a) naturally looks similar to that of the slab without a vacancy — only one atom has been removed (of 56). The effects we are after are local. Looking at the projected DOS (Fig. 4b) for an Fe atom near the vacancy (labelled Fe_{5V} in Fig. 2) and a fully coordinated Fe atom (Fig. 4c) in the same layer (Fe_{6V} in Fig. 2), one may see some similarity to what happens on an Fe(110) surface. The atoms directly neighboring the vacancy are more negative than the remaining Fe atoms of the fourth layer of the slab, and the DOS is somewhat narrowed. The effect is mainly local in nature and the average orbital population for the first Fe neighbors of the vacancy is $d^{6.87}s^{0.67}p^{0.31}$. No change in E_f is observed when the Fe vacancy is introduced.

Regarding the bonding, the COOP curves for the Fe–Fe bulk, surface (average) and near vacancy

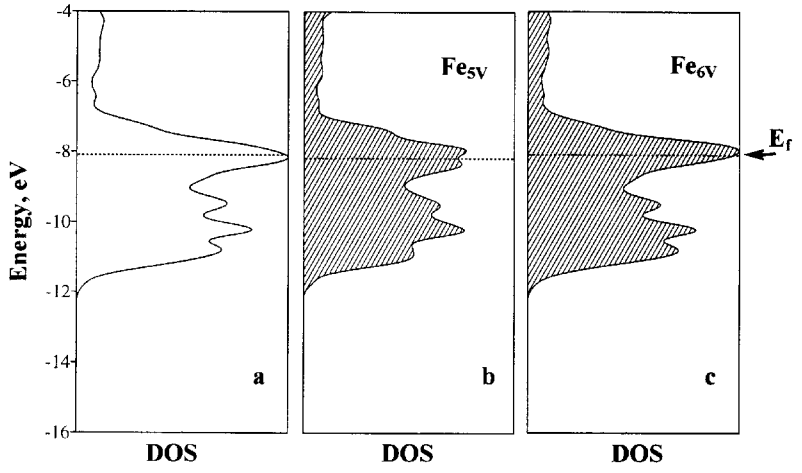

Fig. 4. (a) Total DOS of a seven layer slab with a vacancy in its center at the fourth layer. (b) Projected DOS of an Fe atom first neighbor to the vacancy (Fe_{5V} in Fig. 2) and (c) a bulk-like Fe atom in the same slab (Fe_{6V} in Fig. 2). The contributions of the individual atoms to the DOS (b,c) are scaled arbitrarily to 1/100 of the total DOS (a).

Table 2
Electron densities, overlap populations (OP) and net charges for a seven layer slab of Fe(110) with and without a vacancy

Structure	Electron density				Charge	OP[a]	E_f (eV)
	Total	s	p	d			
3D bulk	8.20	0.66	0.32	7.02	0.000	0.093[b] 0.210[c]	−7.98
First layer (surface)	8.72	0.70	0.29	7.73	−0.720	0.118[b] 0.283[c]	−8.11
Fourth layer (inner)	7.71	0.66	0.32	6.74	0.291	0.095[b] 0.212[c]	—
Fourth layer + vacancy[d]	7.71	0.66	0.31	6.75	0.286	0.097[b] 0.212[c]	−8.10
First neighbor to vacancy[e]	7.85	0.67	0.31	6.87	0.144	0.126[b] 0.240[c]	—
Surface + vacancy[f]	8.68	0.70	0.29	7.68	−0.679	0.146[b] 0.281[c]	—

[a] OP = orbital population.
[b] Fe_{1V}–Fe_{3V} distance: 2.86 Å (see Schemes 2 and 3).
[c] Fe_{1V}–Fe_{2V} distance: 2.47 Å (see Schemes 2 and 3).
[d] Average value.
[e,f] The slab includes a vacancy in its fourth layer.

(average) bonds are similar: the bottom of the d band is metal–metal bonding and the top metal–metal antibonding (see Fig. 5). A similar effect is seen in the s and p band. In the slab, the total Fe–Fe overlap population (OP) for a bond in the innermost layer is 0.210. The OP between surface Fe atoms is 0.283, and between an Fe atom of the first and one of the second layer, 0.265. When a vacancy is introduced, an Fe–Fe bond near the vacancy has an average OP of 0.240. In Table 2 the valence orbital populations, electron densities and charges are summarized.

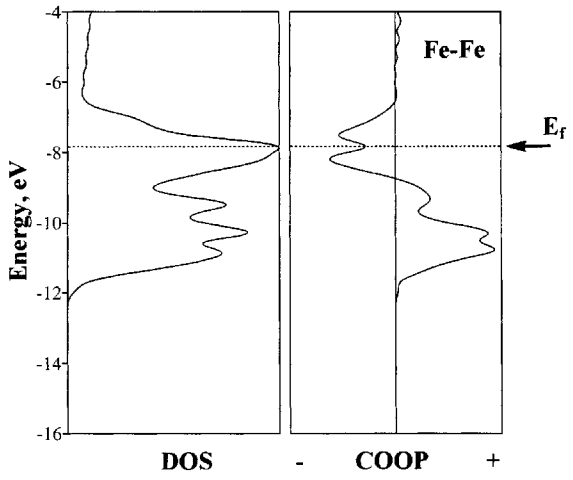

Fig. 5. Projected DOS of the bulk-like (fourth) layer and COOP for an Fe–Fe bulk-like bond of the seven layer slab.

4.1. H on the surface

There are many studies devoted to the chemisorption of atomic H on a metal surface, based on LEED or HREELS measurements [52,53]. The H atom usually occupies a multicenter coordination site on transition metal surfaces, such as a three-fold or a four-fold site. On Fe(110), Moritz et al. have concluded that H is adsorbed at a quasi-three-fold site, with a H–surface distance of 0.9 ± 0.1 Å [43]. In recent experimental studies, Nichtl-Pecher et al. and Hammer et al. have confirmed that H is indeed adsorbed at such a site [54,55]. Both experimental studies [56,57] and theoretical calculations [58,59] have found no significant difference in hydrogen adsorption energy among the long-bridge, short-bridge and quasi-three-fold sites on Fe(110) or W(110).

Cremaschi et al., using ab initio quantum chemical calculations, found the long-bridge adsorption site somewhat more stable than the three-fold site

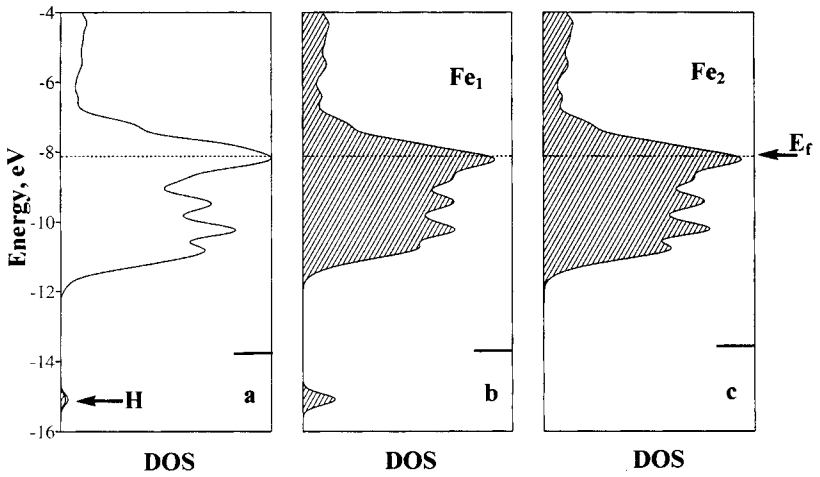

Fig. 6. Total DOS of a seven layer slab with H adsorbed on the Fe(110) surface (long bridge) (a), projected DOS of the Fe surface atoms, first neighbors to H (b) and (c) projected DOS of the Fe second neigbors to H. The bar indicates the H 1s energy before adsorption. The lined region in (a) is the H atom projection.

(by only 0.05 eV [44]). Based on the previous discussion and the similarity in geometry found when H is adsorbed near a vacancy site in Fe (see later), the only surface site studied in this paper was the long-bridge one (see Schemes 3 and 4).

As expected, we found no significant change in the Fermi level. The total DOS is also dominated by the many bulk and surface Fe atoms, so that the changes are subtle. On bonding to the surface, electron transfer occurs from the Fe substrate to H, to the extent of 0.54 e^-, almost twice the value reported by Cremaschi et al. [44]. Fig. 6 left shows the total DOS of the system with the H contribution. The bar on the right in the DOS plots indicates the energy level of the H 1s orbital before interaction.

Analysis of the bonding between H and the surface reveals that the principal contribution to the Fe–H bond is from the H 1s, Fe 4s and 4p orbitals, and to a lesser extent the 3d orbitals. The narrow band of states at -15 eV is composed of 19% 4s, 6% 4p, 7% Fe 3d and 68% H 1s. Thus, the peak at -15 eV is made up of mostly H states, stabilized after adsorption. The H–surface interaction is strong, 29% of the H states are pushed above the Fermi level. Fig. 6b shows the projected DOS for the two Fe of the long-bridge (Fe_1 and Fe_3 in Scheme 3). The peak at -15 eV in the Fe_1 contribution is indicative of the H–Fe interaction; this is where most of the H density is. The DOS for the second neighbor Fe (Fe_2 and Fe_4 in Scheme 3) does not show this peak (see Fig. 6c), and does not differ essentially from an Fe of a clean surface.

As can be seen from Table 3, the H–surface bonding is achieved at the expense of weakening the Fe–Fe surface bond. Thus, the Fe–Fe bond OPs involving Fe atoms directly bonded to H are reduced to 30% of their original value on the clean surface.

Which is the origin of the Fe–Fe bond weakening? This bond weakening is a direct consequence of a strong Fe–H interaction which pushes some Fe–Fe bonding states up to just below the Fermi level. Many states antibonding between metal atoms and empty before chemisorption wind up higher in energy than they were at the outset, but still below the Fermi level after interaction with the H. These levels are populated. The result is that the bonding within the surface is weakened, as attested to by the drop of OP between Fe_1 and Fe_3 (Scheme 3). Comparing the COOP curves for the Fe bonded to H with other Fe–Fe bonds in the surface (Fig. 7), it can be seen that more Fe–Fe antibonding states are occupied when H is near Fe (compare Figs. 7b and 7c and see Table 3).

Table 3
Orbital populations and net charges for a seven layer slab of Fe(110) with H on the surface, near the vacancy and in a tetrahedral interstitial

		Charge	E_f (eV)	OP[a]
H on Fe (110)	Fe_1	−0.541	−8.09	Fe_1–Fe_3 = 0.028[b]
	Fe_2	−0.686		Fe_1–Fe_2 = 0.213[c]
	H	−0.420		Fe_2–$Fe_{4'}$ = 0.107[b]
				Fe_2–$Fe_{1'}$ = 0.281[c]
				Fe–H = 0.286
H–vacancy	Fe_{1V}	0.347	−8.11	Fe_{1V}–Fe_{3V} = 0.037[b]
	Fe_{2V}	0.346		Fe_{1V}–Fe_{2V} = 0.190[c]
	H	−0.355		Fe_{2V}–$Fe_{4V'}$ = 0.082[b]
				Fe_{2V}–$Fe_{1V'}$ = 0.219[c]
				Fe–H = 0.311
H–tetrahedral	Near Fe	0.380	−8.09	Near Fe–Fe = 0.024[b]
				Fe–Fe = 0.153[c]
Interstitial	First Fe	0.362		
	H	−0.288		
				First Fe Fe–Fe = 0.062[b]
				Fe–Fe = 0.221[c]
				Fe–H = 0.297

[a] OP = orbital population. Each bond is identified according to Scheme 1 or Scheme 2.
[b] Fe–Fe distance: 2.86 Å (see Scheme 2Scheme 3).
[c] Fe–Fe distance: 2.47 Å (see Scheme 2Scheme 3).

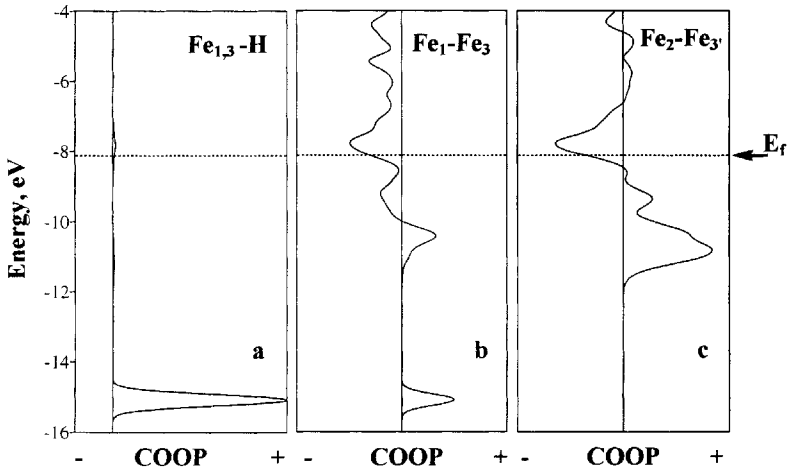

Fig. 7. Fe–H and Fe–Fe COOP curves for Fe(110) surface with H on the long-bridge site. H–$Fe_{1,3}$ (first neighbor) (a) (2×), Fe_1–Fe_3 directly bonded to H (b) and Fe–Fe (second) neighbor to H (c).

Compared with the corresponding inner slab states, the bonding surface states — in the clean Fe surface — are less bonding and the antibonding states less antibonding. For the Fe bulk-like layer, almost all antibonding states are filled. As an antibonding level is in fact more antibonding than the corresponding bonding level is bonding, the loss of antibonding character dominates on the

Table 4
Contribution of the metal orbitals to the hydrogen–iron[a] overlap population[b]

H position	s	p_y	p_z	$d_{x^2-y^2}$	d_{yz}	Total
Surface	0.155	0.038	0.037	0.014	0.042	0.286
Vacancy (minimun)	0.167	0.043	0.022	0.032	0.047	0.311
Vacancy (center)	0.030	0.006	0.010	0.001	0.010	0.047

[a] Calculated for the closest H–Fe distance.
[b] The contributions from orbitals p_x, d_{xy}, d_{xz} and d_{z^2} are zero.

clean surface (see Table 2), causing an increase in the Fe–Fe surface OP. When H is present, the situation changes dramatically, the surface Fe_1–Fe_3 bond gaining antibonding character (see Fig. 7b). There is also less bonding due to greater participation of the Fe 4s orbitals in the H–Fe bonding.

Our calculations are consistent with substantial Fe–H interaction, a hydrogen surface resonance spread out over the Fe s, p and d bands. The decrease in Fe–Fe OP is confined to Fe bonded to H; this can be noted from the negligible changes in OPs for the second nearest surface Fe atoms upon adding H (see Table 3 and Fig. 7c). The orbital contributions to the H–Fe OP are summarized in Table 4. Only the Fe s, p_y, p_z, $d_{x^2-y^2}$ and d_{yz} orbitals participate in the Fe–H bond. In the long-bridge site the H 1s can only interact with the orbitals near the bottom of the s band; the p_x and p_z orbitals lie higher in energy, so the match between them and the H 1s orbital is poor. Regarding the $d_{x^2-y^2}$ and d_{yz} orbitals, even though their overlap with H 1s could be substantial, few such states are occupied and their contribution to the Fe–H OP is small.

4.2. Interstitial H

Let us first discuss the solubility of H in the perfect bcc Fe lattice. Bcc Fe is a poor endothermic absorber of hydrogen; the heat of solution at infinite dilution is 0.20 eV/H atom [60]. The effective medium theory has been successful in describing the energetics of H in metals. Nordlander et al. [12] report excellent agreement for the heat of solution of H in bcc Fe. The impurity interstitial H atom is found to favor a tetrahedral site in most bcc metals (including Fe), while octahedral sites are preferred in fcc metals. This equilibrium position of interstitial hydrogen can be explained in terms of the optimal electron density required in each crystalline structure. The local semi-empirical model of Griessen [10] also predicts the correct site occupancy, in agreement with experimental findings [1–4,61]. Minot and Demangeat [21], using the EH method, studied the location of H in a bcc Fe_2H stoichiometry; they also found the tetrahedral position more favorable when lattice relaxation was included.

In a perfect bcc Fe_{86} cluster (see Fig. 1), we calculated the energetics of H in tetrahedral and octahedral interstitial sites. The ASED-MO method allows us to determine the equilibrium position of H better than the normal extended Hückel procedure. We included relaxation of the first and second Fe neighbor to H (in the tetrahedral interstitial site). Scheme 5 shows roughly the

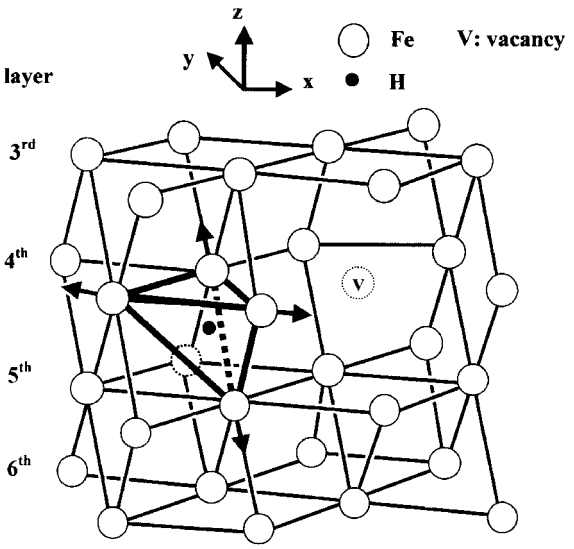

Scheme 5.

movement of the metallic atoms. The lowest energy configuration is found for H located in a tetrahedral interstitial. We do not have a simple orbital explanation for the preference of H for the tetrahedral site. It may be that the lower electrostatic repulsion in this interstitial site is responsible for the H stabilization. The four Fe atoms of this site relax outwards, while the second neighbors find a minimum position relaxing inward but with a displacement one order of magnitude lower than the former. In previous work, Pistonesi et al. studied some asymmetric distortions to the Fe lattice; in any case the symmetric distortion results in a greater stabilization [30].

The H atom (partially anionic, so carrying $\sim 1.4e^-$) thus pushes away the nearest Fe atoms in order to obtain a lower electron density at the site (see Tables 2 and 3). Typically, the lattice expansion around a H atom is of the order of 5%. An empirical rule states that the relative volume expansion of the metal host is approximately 2.9 Å^3 for H in all metals [4]. The actual displacements of the lattice can be thought of as arising from the application of virtual forces (Kanzaki forces) to each lattice atom [20]. Our results, summarized in Table 5, are in qualitative agreement with experimental data and previous simulations [4,20,21].

An analysis of the electronic structure reveals the local nature of the H–Fe interaction at interstitial sites. The H 1s level is shifted down below the bottom of the d band. The main bonding orbital has H 1s and Fe 4s and 3d admixture, while only small changes are observed in the 4p electron density (see Table 3). Electron transfer of nearly $0.3e^-$ from Fe to H occurs, primarily from the first neighbors. The OP values (see Table 3) are also consistent with Fe–Fe bond weakening — the additional electron from the H atom occupies an Fe–Fe antibonding level in the upper part of the d band. It is likely that this factor is important in determining the stability of the lattice around the interstitial H. Similar behavior in the H–Fe interaction at interstitial sites was reported by Itsumi and Ellis [32], although these authors found an electron transfer of nearly $0.6e^-$ toward the H. The lower charge transfer to H found in the present work may be due to an excessive negative charge on the Fe near the defect.

4.3. H near a vacancy

As mentioned in the Introduction, the interaction of H with vacancies and H–H pairing in metals has been studied before, using first principles and semi-empirical calculations [12,26–32]. The results indicate that in general the H–Fe interaction gets stronger when H is close to the vacancy. But the H does not remain exactly at the center of the vacancy, due to a strong indirect interaction mediated by the Fe matrix. The ASED-MO energy minimum occurs at eccentric positions, and when relaxation is included a contraction of 0.32 Å of the first neighbor Fe atoms was reported [12,30]. When no H was present, the contraction was found to be 0.41 Å [30]. Of all H

Table 5
Total energy of the system and effect of lattice relaxation[a]

	Energy (ev)	Lattice relaxation	Volume change (Å^3)
H–vacancy (minimum)	−6.25	First Fe direction: inward displacement: 0.31 Å	1.5
H–vacancy (near octahedral)	−5.90	—	—
H–vacancy (near tetrahedral)	−6.15	—	—
H–interstitial tetrahedral relaxed (perfect lattice)	−5.96	First Fe direction: outward displacement: 0.22 Å	3.2
H–interstitial octahedral relaxed (perfect lattice)	−5.60	—	—
H on the Fe(110) surface	−6.20	—	—

[a] Calculated using ASED-MO and a H–Fe_{86} cluster.

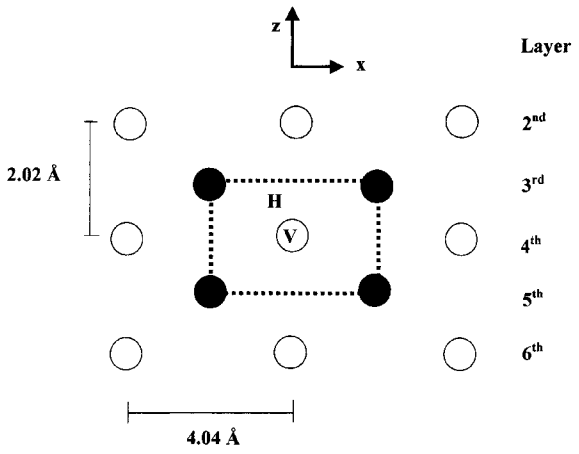

Scheme 6.

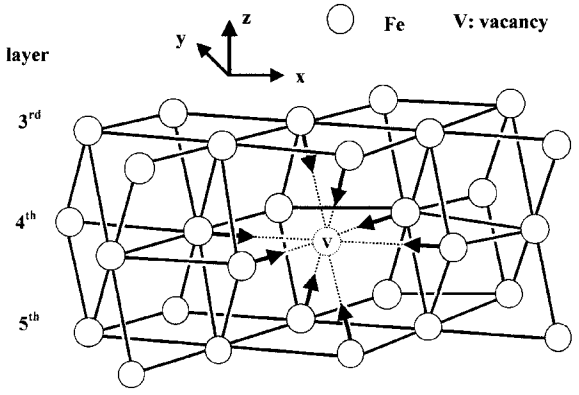

Scheme 7.

locations studied (surface, tetrahedral and octahedral site and vacancy), the vacancy region is the most stable. Schemes 6 and 7 show the H position and the relaxations considered in this region. This preference of H for the bulk region near the vacancy is in agreement with the theoretical results of Nordlander et al., who found that the bonding of hydrogen to vacancies and voids is similar to the bonding at the surface [12]. Upon introducing a vacancy, neighbor Fe atoms develop dangling bonds similar to those at the surface and are more negative than in the perfect lattice (see Table 2). In addition, near the vacancy, H has less repulsive interactions with Fe atoms than in tetrahedral interstitial sites, giving a net increase in the bonding energy. In a very recent study, Curotto et al., using Brownian dynamics and Monte Carlo simulations for the H–Ni clusters, found H most frequently on the surface [62].

The binding energy we obtain of H to the vacancy in Fe_{86} (defined as the difference between the energy of a H atom in the most favorable site of the perfect host metal and that of a hydrogen trapped at a vacancy) is 0.29 eV, somewhat smaller than the experimental value. The local semi-empirical correlation of Griessen gives 0.78 eV, the calculated value from effective medium theory is nearly 1 eV, while the experimental determination is 0.53 eV for this binding energy [10]. In the case of Ni with H, close agreement between theory and experiment is reported by Puska et al. [26].

It can be seen from Fig. 8 that the DOS has a peak at -15.43 eV, which is mainly H 1s stabilized by the H–Fe interaction. This peak represents a state with composition 77% 1s, 16% Fe 4s, 1% 4p and 5% Fe 3d, and is 0.41 eV more stable than the corresponding peak in the DOS for H on the Fe(110) surface (see also Fig. 6). The optimal calculated geometry of the H in a tetrahedral interstitial site displaced 0.25 Å toward the vacancy is close to that of a bridge site on the surface. The electron transfer to the H atom is 0.35 e^-, somewhat smaller than for H on the surface (see Table 3). In the case of bulk metal hydrides, a majority s and p composition for the H–Fe bonding state below the d band has been reported [16,17]. This is also true in our case, as we indicated above; the Fe–H interaction is strong, so that 31% of its states are pushed above the Fermi level. The DOS of the first neighbor Fe atoms (Fe_{1V} and Fe_{3V} in Scheme 2, third layer) and second neighbor (located in the vacancy layer) also show this peak, though with less intensity. This is different from the chemisorption case, where no effect was observed beyond the first neighbor Fe (see Table 3).

Analysis of the bonding between H and Fe at the vacancy confirms that the principal bonding is due to H 1s–Fe 4s interaction (see Fig. 9). As on the surface, the H–Fe bonding is achieved at the expense of weakening the Fe–Fe bond, affecting in this case other near neighbors. From Table 3, the Fe–Fe OP for the Fe directly bonded to H (Fe_{1V}–Fe_{3V} in Scheme 2) diminishes from 0.126 to

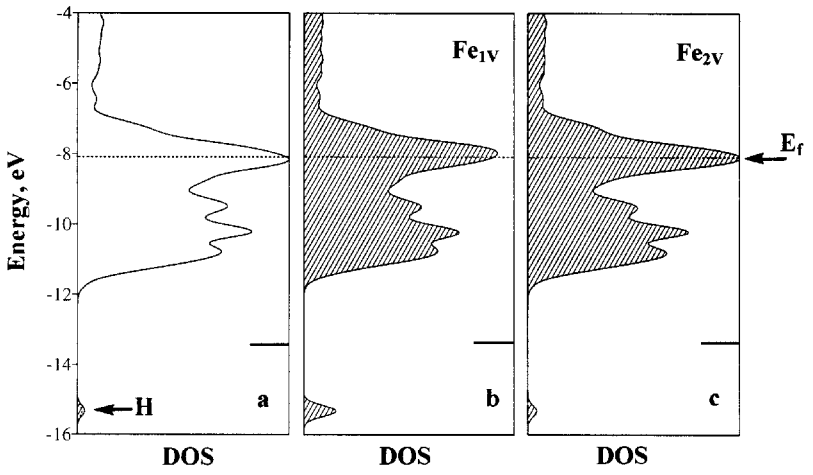

Fig. 8. Total DOS of a seven layer slab with H absorbed in the vacancy region of the Fe slab (see Fig. 1 and Scheme 7) (a), projected DOS of the near vacancy Fe atoms, first neighbors to H (Fe_{1V} and Fe_{3V}) (b) and (c) projected DOS of the Fe second neighbors to H (Fe_{2V} and Fe_{4V}). The bar indicates the H 1s energy before absorption.

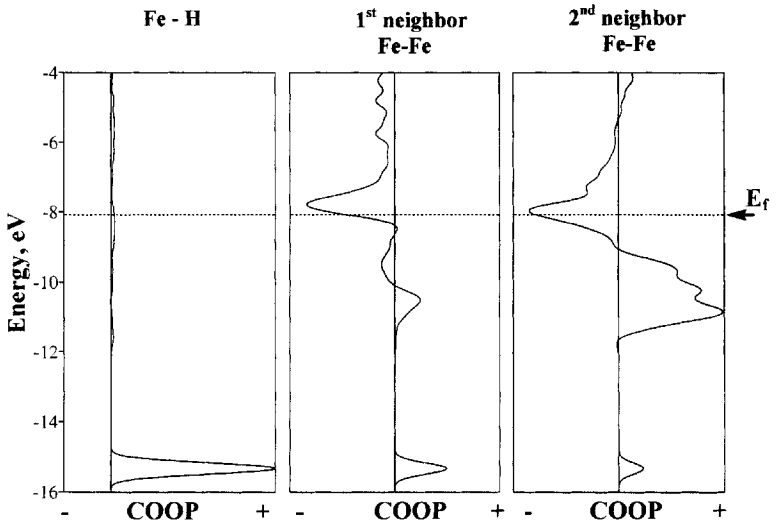

Fig. 9. Fe–H COOP curves for H in the vacancy region. H–Fe, first neighbor (a), Fe–Fe directly bonded to H (b) and Fe–Fe (second) neighbor to H (c).

0.037, and the OP for those Fe–Fe bonds shorter than the former (Fe_{1V}–Fe_{2V} in Scheme 2) from 0.240 to 0.110. The origin of this bond weakening was previously discussed, but the effect seems to be more extended than on the surface, as shown in Fig. 9.

Itsumi and Ellis have reported similar results in the case of H at octahedral distorted sites near a vacancy in bcc Fe [32].

Which is the origin of the detrimental effect of H on the strength of metals? Decohesion is one of the early proposed and most cited mechanisms of H embrittlement [63]. This concept associates embrittlement with a decrease in atomic bond strength, due to the local concentration of H. Recently, Krasko [64] found, by first principles calculations, intergranular decohesion in Fe caused by a H impurity. A hydrogen-like composition for

the stabilized orbital, similar to the one we find, was reported in this work. The orbital contribution to the H–Fe OP is included in Table 4. The same orbitals as those mentioned when H is on the surface take part here, but now the Fe 3d orbital contribution is slightly higher than that of Fe 4p.

5. Conclusions

The electronic structure of H in bcc Fe has been studied by EH tight-binding extended slab and ASED-MO cluster calculations. The following cases were studied: H at the Fe(110) surface, interstitial H located in a perfect lattice and in the neighborhood of an Fe vacancy. The model for the H/Fe system simulates the low solubility of H in Fe. H diminishes the strength of the local Fe–Fe bond to about 30% of its original value. Our results show how the decohesion of Fe–Fe bonds could participate in the embrittlement process. The detrimental effect of H on the Fe–Fe bonds is more extended in the vacancy than on the surface.

The Fe–H interaction occurs mainly via Fe 4s and H 1s orbitals with a small contribution of both 4p and 3d Fe orbitals. The relative participation of 3d orbitals is increased in the vacancy case. H is found negatively charged on the surface and in the lattice, and an Fe–H state is stabilized below the bottom of the d band. The Fe–H bond is formed at the expense of Fe–Fe bonding, and that, rather than an increase in population in antibonding states, is the reason for the mentioned decohesion. Our results are in good agreement with related calculations on Fe surfaces [44], interstitials and vacancies in bcc Fe [6,32] hydride phases [14,17], and recently, vacancy–H interaction in transition metals [28]. Upon introducing a vacancy, neighbor Fe atoms develop dangling bonds similar to those at the surface. The Fe atoms, initially more strongly bonded to each other as a result of vacancy introduction (by depopulation of Fe–Fe antibonding orbitals), diminish their Fe–Fe bond as the new Fe–H bond is formed. The vacancies act as a strong trap for H.

We think this paper contributes to the understanding of H embrittlement by decohesion in metals. Fundamental questions remain to be clarified, such as hydrogen-related phase changes, hydride precipitation and hydrogen-induced local plasticity.

Acknowledgements

The authors acknowledge E. Mershrod for her helpful comments. A.J. is grateful for a FOMEC-FISICA-UNS fellowship, which made possible his stay at Cornell University. Our work was supported by NSF through research grant CHE 94-08455. We are also grateful to the Materials Science Center at Cornell University for its support of this research through grant DMR-9632275.

References

[1] S.M. Myers, M.I. Baskes, H.K. Birnbaum, J.W. Corbett, G.G. De Leo, S.K. Estreicher, E.E. Haller, P. Jena, N.M. Johnson, R. Kirchheim, S.J. Pearton, M.J. Stavola, Rev. Mod. Phys. 64 (1992) 559.
[2] I.M. Bernstein, A.W. Thompson (Eds.), Hydrogen Effects in Metals, AIME, Warrendale, PA, 1981.
[3] N.R. Moody, A.W. Thompson (Eds.), Hydrogen Effects on Material Behavior, The Minerals, Metals and Materials Society, Warrendale, PA, 1990.
[4] Y. Fukai, in: U. Gonser (Ed.), The Metal Hydrogen System, Springer Series in Materials Sciences, vol. 2, Springer, Berlin, 1993.
[5] M. Eberhart, Science 265 (1994) 332 and references cited therein.
[6] F. Besenbacher, S.M. Myers, J.K. Nørskov, Nucl. Instrum. Meth. Phys. Res. B7/B8 (1985) 55.
[7] R.A. Oriani, Acta Metall. 18 (1970) 147.
[8] R.G. da Silva, R.B. McLellan, J. Less-Common Met. 50 (1976) 1.
[9] V.E. Antonov, I.T. Belash, V.F. Degtyareva, E.G. Ponyatovsky, V.I. Shiryaev, Dokl. Akad. Nauk. SSSR 252 (1980) 1384.
[10] R. Griessen, Phys. Rev. B 38 (1988) 3690.
[11] J.K. Nørskov, Phys. Rev. B 26 (1982) 2875.
[12] P. Nordlander, J.K. Nørskov, F. Besenbacher, J. Phys. F 16 (1986) 1161.
[13] J.K. Nørskov, F. Besenbacher, J. Less-Common Met. 130 (1987) 475.
[14] Ch. Opitz, B. Grünler, H. Müller, J. Less-Common Met. 128 (1986) 73.
[15] T. McMullen, M.L. Plumer, M.J. Scott, E. Zaremba, Phys. Rev. B 38 (1988) 1077.
[16] A.C. Zwitendick, Z. Phys. Chem. (Münich) 117 (1979) 89 and references cited therein.

[17] A.C. Zwitendick, J. Less-Common Met. 130 (1987) 249.
[18] C. Demangeat, in: M. Yussouff (Ed.), Lecture Notes in Physics 283, Electronic Band Structure and its Applications, Springer, Berlin, 1987.
[19] H. Adachi, S. Imoto, J. Phys. Soc. Jpn. 46 (1979) 1194.
[20] M. Ruda, D. Farkas, J. Abriata, Phys. Rev. B 54 (1996) 9765.
[21] C. Minot, C. Demangeat, J. Chem. Phys. 86 (1987) 2161.
[22] R.B. McLellan, Z.R. Xu, Scr. Mater. 36 (1997) 1201.
[23] V.G. Gavriljuk, V.N. Bugaev, Y.N. Petrov, A.V. Tarasenko, B.Z. Yanchitski, Scr. Mater. 34 (1996) 903.
[24] V.N. Bugaev, V.A. Tatarenko, K.L. Tsinman, Metall. Nov. Tekhnol. 17 (1995) 32.
[25] B.S. Cao, H. Ichinose, S. Yamamoto, H. Li, Y. Ishida, Philos. Mag. A67 (1993) 1177.
[26] M.J. Puska, R.M. Nieminen, P. Jena, Phys. Rev. B 35 (1987) 6059.
[27] F. Liu, M. Challa, S.N. Khanna, P. Jena, Phys. Rev. Lett. 63 (1989) 1396.
[28] H. Zheng, B.K. Rao, S.N. Khanna, P. Jena, Phys. Rev. B 55 (1997) 4174.
[29] J.-F. Halet, J.-Y. Saillard, C. Koudou, C. Minot, Z. Nomikou, R. Hoffmann, C. Demangeat, Chem. Mater. 4 (1992) 153.
[30] C. Pistonesi, A. Garcia, G. Brizuela, A. Juan, J. Phys. D: Appl. Phys. 31 (1998) 588.
[31] R. Zeller, in: M. Yussouff (Ed.), Lecture Notes in Physics 283, Electronic Band Structure and its Applications, Springer, Berlin, 1987.
[32] Y. Itsumi, D.E. Ellis, J. Mater. Res. 11 (1996) 2206.
[33] R. Hoffmann, W.N. Lipscom, J. Chem. Phys. 36 (1962) 2179.
[34] R. Hoffmann, J. Chem. Phys. 39 (1963) 1397.
[35] M.-H. Whangbo, R. Hoffmann, J. Am. Chem. Soc. 100 (1978) 6093.
[36] G. Landrum, Yet Another Extended Hückel Molecular Orbital Package (YAeHMOP), Cornell University, 1997. YAeHMOP is freely available on the World Wide Web at: http://overlap.chem.cornell.edu:8080/yahemop.html
[37] J.H. Ammeter, H.-B. Bürgi, J.C. Thibeault, R. Hoffmann, J. Am. Chem. Soc. 100 (1978) 3686.
[38] R. Ramirez, M.C. Böhm, Int. J. Quantum Chem. 30 (1986) 391.
[39] R. Ramirez, M.C. Böhm, Int. J. Quantum Chem. 34 (1988) 571.
[40] A.B. Anderson, J. Chem. Phys. 62 (1975) 1187.
[41] R. Hoffmann, Solids and Surfaces: A Chemist's View of Bonding in Extended Sructures, VCH, New York, 1988.
[42] N.W. Ashcroft, N.D. Mermin, Solid State Physics, Saunders College, Philadelphia, 1976.
[43] W. Moritz, R. Imbihl, R.J. Behm, G. Ertl, T. Matsushima, J. Chem. Phys. 83 (1985) 1959.
[44] P. Cremaschi, H. Yang, J.L. Whitten, Surf. Sci. 330 (1995) 255.
[45] D.E. Lide (Ed.), Handbook of Chemistry and Physics, CRC Press, Boca Raton, FL, 1997.
[46] J.-Y. Saillard, R. Hoffmann, J. Am. Chem. Soc. 106 (1984) 2006.
[47] D.A. Papaponstantopoulus, Handbook of Band Structures of Elemental Solids, Plenum Press, New York, 1986.
[48] E. Shustorovich, R.C. Baetzold, J. Am. Chem. Soc. 102 (1980) 5989.
[49] E. Shustorovich, J. Phys. Chem. 86 (1982) 3114.
[50] P.J. Feibelman, D.R. Hamann, Solid State Commun. 31 (1979) 413.
[51] M.C. Desjonqueres, D. Spanjaard, D. Lassailly, C. Guillot, Solid State Commun. 34 (1980) 807.
[52] K. Christmann, Surf. Sci. Rep. 1–3 (1988) 9 and references cited therein.
[53] M.A. Van Hove, S.Y. Tong, Surface Crystallography by LEED, vol. 2, Symposium Series in Chemical Physics, Springer, Berlin, 1979.
[54] W. Nichtl-Pecher, J. Gussann, L. Hammer, K. Heinz, K. Muller, J. Vac. Sci. Technol. A10 (1992) 501.
[55] L. Hammer, H. Landskron, W. Nichtl-Pecher, A. Fricke, K. Heinz, K. Muller, Phys. Rev. B 47 (1993) 15969.
[56] F. Bozzo, G. Ertl, M. Grunze, M. Weiss, Appl. Surf. Sci. 1 (1997) 103.
[57] R. Imbihl, R.J. Behm, K. Christmann, G. Ertl, T. Matsushima, Surf. Sci. 117 (1982) 257.
[58] T.J. Raeker, A.E. DePristo, Surf. Sci. 235 (1990) 84.
[59] P. Nordlander, S. Holloway, J.K. Nørskov, Surf. Sci. 136 (1994) 59.
[60] M. Puska, R. Nieminen, Phys. Rev. B 29 (1984) 5382.
[61] H.D. Cartajen, Phys. Status Solidi A 59 (1980) 11.
[62] E. Curotto, A. Marco, D.L. Freeman, J.D. Doll, J. Chem. Phys. 108 (1998) 729.
[63] E.A. Steigerwald, F.W. Schaller, A.R. Troiano, Trans. Metall. Soc. AIME 218 (1960) 832.
[64] G. Krasko, Mater. Sci. Eng. A 234 (1997) 1071.